Probing the Conformational Distributions of Subpersistence Length DNA

Alexander J. Mastroianni,[†§] David A. Sivak,[‡] Phillip L. Geissler,[†§] and A. Paul Alivisatos[†§*]
[†]Department of Chemistry and [‡]Biophysics Graduate Group, University of California, Berkeley, California; and [§]Materials Sciences Division, Lawrence Berkeley National Laboratory, Berkeley, California

ABSTRACT We have measured the bending elasticity of short double-stranded DNA (dsDNA) chains through small-angle x-ray scattering from solutions of dsDNA-linked dimers of gold nanoparticles. This method, which does not require exertion of external forces or binding to a substrate, reports on the equilibrium distribution of bending fluctuations, not just an average value (as in ensemble fluorescence resonance energy transfer) or an extreme value (as in cyclization), and in principle provides a more robust data set for assessing the suitability of theoretical models. Our experimental results for dsDNA comprising 42–94 basepairs are consistent with a simple wormlike chain model of dsDNA elasticity, whose behavior we have determined from Monte Carlo simulations that explicitly represent nanoparticles and their alkane tethers. A persistence length of 50 nm (150 basepairs) gave a favorable comparison, consistent with the results of single-molecule force-extension experiments on much longer dsDNA chains, but in contrast to recent suggestions of enhanced flexibility at these length scales.

INTRODUCTION

The bending elasticity of double-stranded DNA (dsDNA) at short length scales matters crucially in many biological contexts. In settings as diverse as eukaryotic nucleosomal compaction, viral genome packaging, and transcription regulation, dsDNA is sharply bent over tens to hundreds of basepairs (bp). Thus, the precise nature of its bending elasticity strongly affects the energetics of many biological processes (1).

Furthermore, the ability of DNA to encode information in a thermally stable double strand that can be as short as four nanometers has led to extensive study of the use of DNA as a building block in artificially programmable nanoscale assemblies. In pioneering work, Sherman and Seeman showed that carefully designed sequences spontaneously form multiple interlocking DNA strands, which adopt complex shapes and symmetries (2). The use of oligonucleotides to direct the assembly of arrangements of nanoparticles has now been studied for more than a decade: Mirkin et al. (3) showed that gold nanoparticles with a surface saturation of attached oligonucleotides can be assembled into arrays stabilized by hybridization of complementary linker strands.

A related set of experiments involves the DNA-directed assembly of nanocrystal molecules (4–8) in which a discrete and specific group of nanoparticles is joined together by oligonucleotides. These nanocrystal molecules are model systems for nanoscience, as they allow the study of interactions between controlled numbers of nanoparticles in groupings of increasing compositional and spatial complexity. This has already been exploited in experiments in which changes in the coupling between surface plasmons on the metal nanoparticles were exploited as a plasmon ruler to study the time-resolved behavior of DNA when it is cleaved by a restriction enzyme (9). The bending flexibility of the DNA strongly influences the resulting structures. The study and application of these nanocrystal molecules hinge on understanding the mechanical properties of the intervening dsDNA, much as the chemistry of conventional molecules depends on a thorough understanding of covalent bonds.

The most quantitative mechanical information about dsDNA bending elasticity has come from single-molecule force-extension measurements performed with optical or magnetic tweezers on long strands of λ-phage genomic dsDNA. These studies have shown that dsDNA can be described accurately on the kilobase scale as a wormlike chain (WLC), a fluctuating elastic filament inextensible along its contour. Mechanical response in this model is governed by a single microscopic parameter, the persistence length ℓ_P ~50 nm (~150 bp) (10,11), which sets the contour length scale over which orientational correlations decay. Thermal fluctuations of a WLC with $\ell_P = 50$ nm have also been used to accurately predict the rates of cyclization of medium-length (100s of bp) dsDNA chains in ligation experiments (12).

It has been suggested, however, that oligomers shorter than a single persistence length may be considerably more flexible than a WLC with $\ell_P = 50$ nm. Measuring the end-to-end distance of DNA free in solution by fluorescence resonance energy transfer and its radius of gyration by small-angle x-ray scattering (SAXS), Yuan et al. have inferred an effective persistence length of 20 nm for chains comprising fewer than 21 bp (13). (These experiments primarily probed DNA up to 21 bp, and the longest strand used—89 bp—may have been intrinsically flexible due to sequence effects.) Furthermore, dsDNA ligation experiments by Cloutier and Widom on chains of modest length (~100 bp) have measured cyclization rates much higher than those of corresponding WLCs with $\ell_P = 50$ nm (14), though others report similar experiments closely matching

Submitted April 6, 2009, and accepted for publication June 11, 2009.

Alexander J. Mastroianni and David A. Sivak contributed equally to this work.

*Correspondence: alivis@berkeley.edu

Editor: Laura Finzi.

0006-3495/09/09/1408/10 $2.00

doi: 10.1016/j.bpj.2009.06.031

47 nm WLC predictions (15). As a potential resolution of these observations, Wiggins et al. have shown that many microscopic models of dsDNA bending yield the response of a WLC with $\ell_P = 50$ nm at large scales while differing in the local details of bending energetics (16).

In this article, we seek to address the following issue: does the WLC model for dsDNA remain accurate in describing equilibrium bending fluctuations on length scales of tens of nanometers, or are more detailed energetic considerations necessary to capture its mechanical behavior? We present experimental interrogation and theoretical explanation of the equilibrium ensemble of end-to-end distances for dsDNA chains significantly shorter than their persistence length. We prepared gold nanoparticle dimers consisting of two particles connected by a single piece of dsDNA, of length 42–94 bp, and then used SAXS to measure the thermal distribution of interparticle distances in these solutions. X-ray scattering experiments have previously measured the arrangement of polymer subunits of DNA chains in solution (not conjugated to nanoparticles), to infer intrastrand and interstrand potentials (17–19). In our study the electron-dense gold nanoparticles dominate the scattering, and thus the resulting pattern of scattering intensity reflects the distribution of inter-nanoparticle distances, and indirectly the distribution of DNA end-to-end distances.

To interpret these experiments we compared with results of Monte Carlo (MC) simulations for dsDNA bending models with single-basepair resolution. We find that the simple WLC model with a standard persistence length of $\ell_P = 50$ nm is quite accurate in describing dsDNA conformational statistics for constructs comprising tens of basepairs. We regard the success of this simple semiflexible polymer model as an indication that correlations in local bending angle (in contrast to those in local orientation) do not extend much beyond a few bp. Our computer simulations highlight the consequences of such a limited correlation length: for chain conformations determined by tens of statistically independent bending angles, even highly nonlinear elaborations in bending potential (e.g., those proposed to describe disruption of local basepairing) influence distributions of typical end-to-end distance fluctuations in barely perceptible ways, provided they are consistent with the well-established mechanics of dsDNA at large scales. The computational results we present are thus robust to changes in the fine details of bending energetics. They are quite sensitive, however, to the way certain aspects of the DNA-nanoparticle attachment geometry are treated, emphasizing the importance of scrutinizing how indirect measurement methods report on macromolecular structure at the nanometer length scale.

EXPERIMENTAL METHODS

Sample preparation

We prepared our dimers using established techniques for DNA-nanoparticle conjugation (20,21) (see Experimental Methods in the Supporting Material for details). We first conjugated gold nanoparticles to single-stranded DNA via a thiol linker at the 5′ end, then further passivated the surface with carboxy-terminated thiolated PEG oligomers. Next we used gel electrophoresis to separate and collect monoconjugates (gold bearing just one single-stranded DNA ligand). We did the same with a complementary strand of DNA, and then mixed the two to produce our dimers (pairs of gold nanoparticles tethered by a single piece of dsDNA). We prepared solutions of the dimers in 0.5× tris-borate-EDTA buffer, at a concentration of 0.5 μM. The ionic strength was raised to 100 mM by the addition of 1 M NaCl in the tris-borate-EDTA buffer. In previous studies we have prepared samples with divalent cations (Mg^{2+}, Ca^{2+}) present (9). However, the particles are not stable in the presence of these divalent ions at comparable ionic strengths to those prepared with Na^{+}. Although further stability could be achieved with a more substantial PEG coat, we chose to avoid this potential perturbation in this study.

We used DNA ranging from 42 to 94 bp, in alternating 10- or 11-bp increments. Given the 10.5-bp helical repeat of B-DNA (22), this preserves the helical phasing between the 5′ ends, and thus between the gold nanoparticles. The lower bound of 42 bp is the practical limit of our purification process, as the electrophoretic bands become more closely spaced with short DNA (though recent advances in monoconjugate purification should permit shorter DNA in future experiments (23)). The upper bound of 94 bp reflects synthetic challenges, and at the extreme, kilobase-long viral genomic DNA would push the measured distances beyond the Nyquist limit of our SAXS instrument. (For DNA sequences, see Sequences in the Supporting Material.)

SAXS measurements

We carried out our SAXS measurements in the same manner as in previous, similar experiments (7–9). Each sample was prepared in a 20 μL aliquot, and flamesealed in a 2.0 mm diameter quartz capillary. Based on the diameter of our x-ray spot, the thickness of the capillary, and the concentration of our solution, a typical experiment samples ~7.5×10^{16} dimers. Data were collected from each sample for 5 h. As standards, we collected data from solutions of bare-gold nanoparticles (lacking any attached DNA strand) in the same concentration and ionic strength.

Our instrumental geometry allows collection of scattered energy up to scattering angle $2\theta = 3^\circ$. We report our scattered intensity as a function of the magnitude of the scattering vector $|\vec{q}| = \frac{4\pi}{\lambda}\sin\theta$, for wavelength $\lambda = 1.54$ Å. Taking into account the finite size of our detector, and the beamstop, which protects the detector face from the primary beam, our measured q-range is 0.013–0.213 $Å^{-1}$. (For further details of the instrumentation, see Experimental Methods in the Supporting Material.)

Even for our longest dsDNA length, the volume occupied by each dimer (assuming a sphere defined by free rotation about a dimer's center of mass) is roughly 1% of the average volume per dimer at our solution concentration, preventing scattering between nanoparticles from different dimers, and making the modeling assumption of infinite dilution a reasonable approximation.

EXPERIMENTAL RESULTS

Scattering data in reciprocal space

By performing SAXS measurements on samples of bare-gold nanoparticles we measure the scattering form factor $P(q)$ of the nanoparticles, convolved with their size distribution, and slightly broadened through further convolution with instrumental effects such as the finite size of the beam. The scattering we measure for DNA-nanoparticle conjugates is the product of this effective form factor and a structure factor $S(q)$, the Fourier transform of the spatial distribution function of the particles. We calculate these structure factors by dividing experimental SAXS data $I(q)$

from each dimer sample by experimental data from bare-gold nanoparticles, prepared in the same concentration and ionic strength (Fig. 1). The measured structure factors qualitatively show an increasing nanoparticle center-to-center distance (our experimental observable) with increasing dsDNA length. However, these experimental structure factors do not fit the simple formula, $S(q, D) = 1/2\ \sin(qD)/(qD) + 1/2$, for two particles separated by a fixed distance D, immediately implying significant variations in interparticle distances.

Transformation to real space

Although reciprocal space data contain all measured structural information, gleaning physical intuition from this format is difficult. To gain intuition about our system, we transformed our data into real-space pair distribution functions, $p(r)$, by generalized indirect Fourier transformation (GIFT) (24) with the program GNOM (25). We observe two peaks in these data: the first, identical to that from solutions of bare gold, arises from scattering from an isolated nanoparticle; the second peak is the result of interparticle scattering events, and thus manifests the distribution of distances between the particles. From these data we see that the particles become farther apart and explore a greater distribution of distances with increasing DNA length, as expected (Fig. 2). These data are, however, subject to artifacts due to transformation from a finite q-range. Where GIFT produces negative probability, we truncate the density to zero, and calculate the mean distances by integration over the second peak. Thus, these data are offered for intuitive value but the formal fitting of our model is carried out on the reciprocal space data, which are free of these potential artifacts. (See Indirect Fourier Transformation, as well as Experimental Means in the Supporting Material.)

Experimental controls

We sought to rule out any significant perturbation of the material of interest, DNA, due to our nanoparticles and measurement apparatus. Significantly, the gold nanoparticles occupy substantially more volume than the dsDNA chain. As such, we conducted several controls and comparisons to previous experiments.

The dynamics of conformational fluctuations are certainly influenced by the relatively large gold nanoparticles tethered to the dsDNA, due to the drag associated with moving them through solution and to more complex hydrodynamic effects coupling the mutual motion of gold and DNA. Static properties of the chain at thermal equilibrium, however, are completely insensitive to these consequences of solvent flow (as ensured by the statistical independence of velocities and configurations in classical systems governed by the Boltzmann distribution).

The excluded volume of the gold nanoparticles in general may exert a stretching force on the DNA molecule, by preventing bent conformations that would otherwise bring the nanoparticles into overlap with each other. This type of behavior has been analyzed for tethered particle motion experiments (26). However this effect should be vanishingly small in our constructs, due to the relatively small size of the gold nanoparticles (much smaller than optical beads in tethered particle motion) and stiffness of DNA (because of its short contour relative to its persistence length). Indeed, control simulations that allow gold-gold overlap are essentially indistinguishable from those with a full volume-exclusion model. The nanoparticles may nonetheless contribute to the reversible work required to change the chain's end-to-end distance, most likely through steric or electrostatic interactions between DNA and the nanoparticles or their alkane tethers. We have also examined these interactions in computer simulations and found them to have negligible effects on DNA bending statistics. In any event, gold-gold and gold-DNA volume exclusion is accounted for in our simulations, and thus should not lead to artifacts in interpretation of experimental structure factors.

Another concern is the effect of interactions at the ends of the double helix. We designed sequences that begin and end with 10 bp of guanine and cytosine residues only, intended to minimize fraying at the ends. These same end sequences

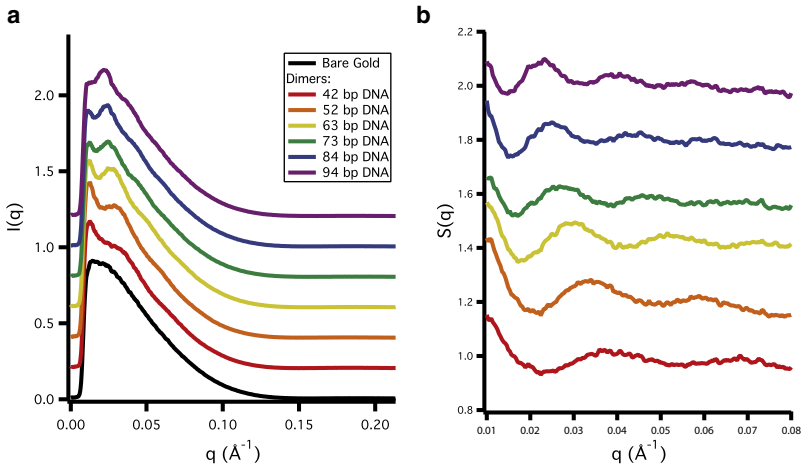

FIGURE 1 Experimental SAXS data in reciprocal space. Ordinates are presented in arbitrary units. All traces are given a constant offset for clarity. (*a*) Raw data for dimers with all lengths of DNA and bare gold. (*b*) Structure factors calculated by division of dimer data by bare gold data.

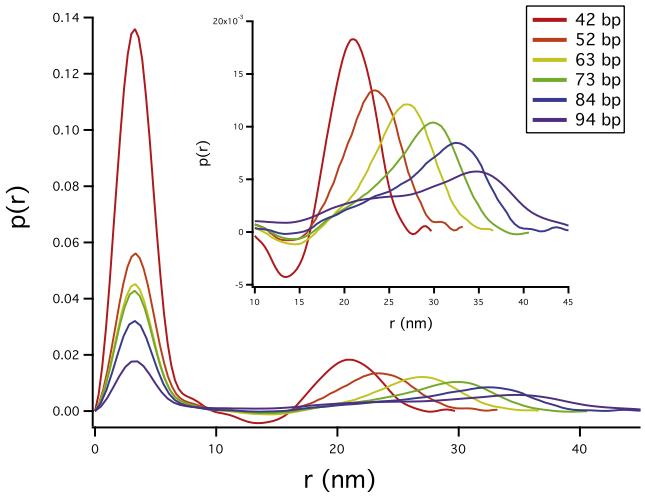

FIGURE 2 Pair distribution functions calculated with indirect Fourier transformation. (*Inset*) Detail of dimer peak arising from interparticle scattering. In these data, the artifacts of Fourier transformation are apparent in the form of negative probability distribution and oscillations near the base line.

were used in all dsDNA in the experiment to control for interactions between the particles and the dsDNA.

We passivated the nanoparticles with a carboxy-terminated polyethylene glycol surface for enhanced salt stability. We also carried out control experiments with dimers that lacked this polymer shell and simply had a bis(*p*-sulfanatophenyl)phenyl-phosphine coating, a smaller, more weakly bound ligand. The presence of a different passivating coat did not significantly affect the shape of the distance distribution, but merely shifted the peak by ~1 nm, as would be expected from a thinner ligand shell and lesser particle excluded volume (see Choice of Nanoparticle Ligands in the Supporting Material).

Previous experiments used similar gold nanoparticle-dsDNA dimers as substrates for enzymatic activity: in one case, dark-field light scattering monitored interparticle distance during *Eco*RV cleavage of dsDNA containing an appropriate recognition sequence (9); in a second experiment, T4 *Taq* ligase covalently linked monoconjugates, as verified by electrophoresis, electron microscopy, and SAXS (7). In both cases the enzymes acted on DNA tethered to gold nanoparticles as on free DNA, so we generally rule out severe perturbations of the DNA by the gold nanoparticles.

Heating and damage from the x-ray beam is unlikely because our x-ray energy (8 KeV, copper Kα) is not resonant with elements in our samples. To further rule out this possibility, we measured the temperature in the sample chamber by preparing a capillary of gold colloid in the usual manner, and adding a thermocouple with the junction in the solution. During a test run, the temperature ranged from 19.8°C to 20.4°C with an average of 20.1°C. Furthermore, were local nanoparticle heating a concern, we would destroy our samples by the loss of thiol bonds and be unable to observe dimers after repeated scans. In previous temperature-dependent scans we noted loss of dimer product at temperatures as low as 35°C; when we scanned dimer samples repeatedly for 900 s, we observed no change in SAXS signal, giving us confidence that the dimers remain stable over the course of multiple runs.

COMPUTATIONAL METHODS

Coarse-grained modeling

Distortions in the internal structure of one segment of a dsDNA chain can influence internal distortions in other segments only within a limited range of contour length, λ. We refer to this length scale λ as the bending correlation length, as opposed to the (orientational) persistence length ℓ_P. With the melting transition distant by at least 20°C (estimated from DINAMelt server (27)), there is little a priori reason to expect that λ should much exceed 1 nm: the hydrophobic, electrostatic, and hydrogen-bonding interactions mediated by solution extend only over $\lesssim$1 nm, while the width of the double helix itself is ~2 nm. Our physical picture of an oligomer tens of nm in contour length is thus a series of several independently bending segments. It is the small magnitude of such local bending fluctuations that causes the chain's orientation to persist over much larger scales.

We assume in our modeling a bending correlation length of $\lambda = 1$ bp. Although this value almost certainly underestimates the bending correlation length of dsDNA, the results we present are insensitive to a 10-fold increase (see Link-Length Insensitivity in the Supporting Material). We thus write a chain's bending energy as a sum over a discrete set of N noninteracting basepairs,

$$E_{\text{bend}} = \sum_{\text{basepairs } i}^{N} \epsilon_i.$$

Correspondingly, the conformation of an oligomer is represented by a linear chain of $N + 1$ bond vectors $\mathbf{b}_i$ (see Modeling Bending Elasticity in the Supporting Material), with end-to-end separation

$$\mathbf{R} = \sum_i \mathbf{b}_i.$$

Alignment of consecutive vectors determines the local bending energy ϵ_i.

We employ a simple WLC model of local bending. Although this model almost certainly oversimplifies the mechanics of dsDNA distortions at the single-basepair level, the results we present are insensitive to any reasonable additional complication in the bending potential. We satisfy the WLC constraint of inextensibility by fixing the length of each bond vector, $\mathbf{b}_i = d\hat{t}$. Here, $\hat{t}$ is a unit tangent vector and $d \approx 0.34$ nm (22) for B-DNA. Energy in this model is a quadratic function of local curvature,

$$\epsilon_i = \frac{k_B T\, \ell_P}{d}|\kappa_i|^2,$$

where

$$\kappa_i = \hat{t}_{i+1} - \hat{t}$$

Succinctly, the internal energy of our dsDNA oligomers is

$$E = E_{steric} + E_{bend} = E_{steric} + k_B T \frac{\ell_P}{d} \sum_{basepairs\ i} (1 - \cos\theta_i)$$

for local bending angle

$$\theta_i = \cos^{-1}(\hat{t}_{i+1} \cdot \hat{t}_i)$$

(see Fig. S4 *A* in the Supporting Material). E_{steric} is a hard-core potential that prevents different segments of the chain from overlapping, as described below. This steric contribution has almost no effect on the short chains we consider here. We include it for physical consistency with our treatment of the gold-DNA junction. Aside from the ineffectual constraint of self-avoidance, this model is nothing more than a discretized version of WLC models that so successfully capture dsDNA response at much larger scales.

Because x-ray scattering probes the spatial arrangement of gold nanoparticles, rather than the extension of dsDNA itself, we have paid careful attention to the structure and consequences of the gold-DNA attachment. Although this junction is subnanometer in scale, the constraints it introduces have a profound influence on theoretical predictions. The structure of our model dimer system is sketched in Fig. 3 *a*.

The discussion above might seem to suggest that there is no significant need to resolve the double-helix structure of dsDNA at all. For bending at the length scales of interest, we indeed argue that such detail is unimportant. But in describing the gold-DNA junction, its consideration becomes crucial. The alkane linkers are sufficiently short that their point of attachment to the dsDNA helix can dramatically affect the volume accessible to the gold nanoparticles (see Fig. 4). Treating the linkers simply as continuations of the discrete dsDNA WLC, albeit with different segment length and persistence length, would effectively attach them to the middle of the dsDNA helical axis. Chemically, however, they are covalently bound to the phosphate backbone, which spirals along the outside of the circumscribing cylinder.

For the purpose of describing this attachment geometry, we add to our model an explicit representation of the phosphate backbone. We do so by introducing a twist degree of freedom for each basepair to represent the phosphate backbone of one strand, with the other strand's phosphate backbone at a fixed angle reflecting the major-/minor-groove asymmetry, though our results do not change when this asymmetry is neglected.

In the model we attach the alkane linkers to the backbones. This chemically appropriate attachment produces a marked shortening in the experimentally observable distance between gold nanoparticles. Although gold and DNA both possess a dimension much larger than the intervening junction, changes in its microscopic structure in effect modify boundary conditions dictating the volume around the oligomer that is accessible to the tethered nanoparticles.

Alkane linkers between the 5′ phosphate group and the nanoparticle-bound thiol are modeled as discrete chains with their own WLC bending potential, with a persistence length of 0.5 nm (28). Gold particles are represented explicitly, but have only connectivity interactions with the adjacent linker and excluded volume interactions with the entire chain. The passivating coat of PEG is modeled as a volume-excluding shell of width 0.5 nm surrounding the gold nanoparticle (Fig. 3 *a*).

Given the limited resolution of our model, excluded volume of the dsDNA helix is difficult to capture in great detail. In the crudest approach, we associate a hard sphere with each dsDNA basepair (centered on the helical axis) to represent the width of the double helix. Here, the shape of the chain's termini is most faithfully represented if the final basepair on each end does not exclude volume. These excluded volume interactions are crucial to prevent significant overlap between gold nanoparticles and the dsDNA helix, which would otherwise be significant due to the extreme flexibility of the alkane linkers. We implemented as well a more detailed steric model based on the positions of phosphate backbone nodes (each excluding a sphere of radius 0.05 nm), replacing the volume exclusion previously positioned on the dsDNA centerline. This additional detail had no significant effect on the distributions $p(r)$ (see Volume Exclusion in the Supporting Material). In the context of the experiments we have performed, the site of linker attachment appears to be the single salient subnanometer feature of the tethered-nanoparticle constructs.

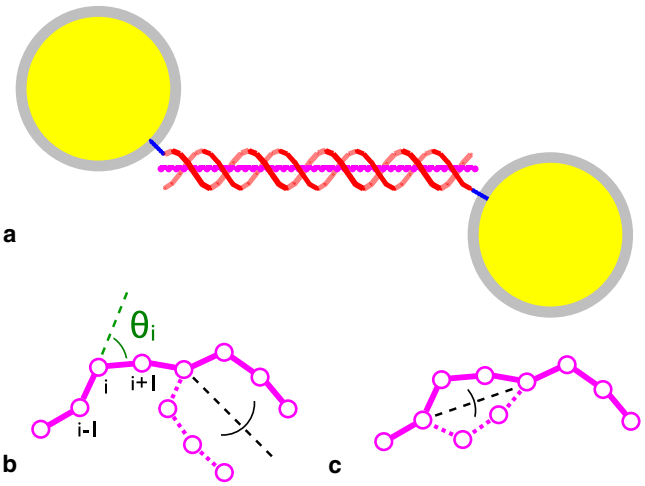

FIGURE 3 (*a*) Model schematic. dsDNA helical axis nodes (*purple*) and alkane linker nodes (*blue*) carry bending elasticity; dsDNA backbone nodes (*red*) rotate around the helical axis subject to twist-elastic energetics. Moves for conformational sampling: (*b*) free rotations; (*c*) crankshaft rotations. Backbone nodes have been omitted for clarity in *b* and *c*.

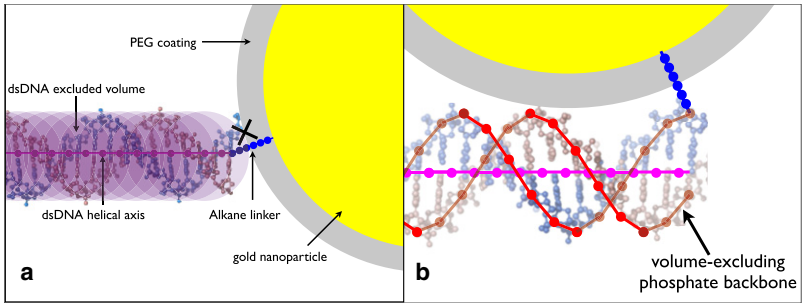

FIGURE 4 Details of linker attachment to dsDNA helix significantly affect volume accessible to gold nanoparticles. (*a*) End attachment prevents gold nanoparticles from sampling volume on the sides of the dsDNA helix. (*b*) Side attachment allows gold nanoparticles to come into much closer proximity.

Conformations of our model dsDNA chains are sampled from a Boltzmann distribution using MC importance sampling with the standard Metropolis acceptance criterion. We employ several kinds of trial moves (see Fig. 3, *b* and *c*, and Moves in the Supporting Material for details) to efficiently navigate this canonical ensemble.

Generating results for comparison with experiment

Our MC simulations produce a distribution of distances between centers of gold nanoparticle pairs. We Fourier-transform the real-space distribution to generate a simulated structure factor. For comparison in reciprocal space, we linearly shift the simulated structure factor to match the average value of the experimental structure factor over the range unlikely to be subject to experimental artifact (0.013–0.04 Å), and we multiplicatively scale this shifted simulated structure factor to match the mean-squared deviation of the experimental structure factor over that same range. The average value and mean-squared deviation correspond roughly with the concentration and dimerization efficiency, respectively—quantities difficult to measure experimentally. (The relative quantities of bare-gold and dimers can be measured by the optical density of their bands in gel electrophoresis, or by counting particles with electron microscopy, but the necessary sample preparations for these techniques break some portion of the thiol bonds and lead to inaccuracy.) For a real-space comparison we multiply the raw simulated structure factor by the experimentally measured scattering form factor $P(q)$ of gold nanoparticles without any attached DNA (containing the relevant polydispersity and instrumental broadening). We then invert the Fourier transform to a pair distribution function $p(r)$. (See Comparing Theory and Experiment in the Supporting Material.)

Whereas qualitatively similar conclusions follow from comparisons in real- or in reciprocal-space, the reciprocal-space comparison is more direct, as the data are not affected by potential artifacts from the GIFT algorithm, applied to a limited q-range. In particular, there is a noticeable discrepancy between the simulated and experimental real-space pair distribution functions for the longest dsDNA chains at low separations. This shoulder appears to be an artifact of the GIFT protocol: simulated distributions, excised of low-q data and then transformed to real-space using GIFT, show a similar shoulder for the same lengths of dsDNA. We present the real-space comparisons for the clarity of their physical insights, but draw our conclusions quantitatively from the reciprocal-space fits.

RESULTS AND DISCUSSION

Experimental support for the coarse-grained model

A semiflexible polymer is often caricatured as being rigid on length scales smaller than a persistence length. Calculations based on this notion highlight its quantitative inaccuracy: if instead of allowing bend fluctuations we treat dsDNA as a rigid rod, then we predict mean gold-gold distances at significantly greater extension than those observed experimentally (see Experimental Means in the Supporting Material). This confirms our physical intuition that thermal excitations play an important role in this system, and that modeling equilibrium fluctuations is necessary to capture the dsDNA behavior seen in these experiments.

The sequence-dependence of dsDNA thermal excitations on very short length scales is well established: dinucleotide-specific dsDNA elasticity parameters have been derived from structural databases (29); and the propensity for base-pairs to melt is strongly sequence-dependent (30). For each length of dsDNA we used three different internal sequences, with the central 22–74 bp of each a random sequence containing 40%, 50%, or 60% GC residues. We rejected sequences containing regions known to markedly affect the strand's conformation, such as A-tracts (31,32), G-quartets (33), or sequences forming stable hairpins or self-dimers. We found no systematic differences between our chosen sequences, however, so in this work we focused exclusively on the 50% GC content samples. (This relative insensitivity of our experimental observable to sequence variation is not surprising; see Sequence Insensitivity in the Supporting Material for further discussion.) This sequence-insensitivity pointed us toward a sequence-independent model that does not resolve individual base differences.

We also prepared each sample with four different ionic strengths, 50, 100, 200, and 400 mM. Within this range there were no discernible differences in our experimental data,

consistent with empirical studies (34) that predict a variation in persistence length of only ~2.5 nm over this range of monovalent concentration. We thus focus here on the 100-mM ionic strength samples, and conclude that more careful modeling of these effects is unlikely to produce added explanatory power. (See Experimental Means as well as Sequence and Salt Variation in the Supporting Material.) While we have exclusively studied solutions containing monovalent cations in this work, others have studied the effect of divalent and trivalent cations on dsDNA (34). These multivalent cations have been found to produce short-range attractive potentials between dsDNA segments (35,36), and this could be an interesting topic for future studies.

Best fit and quality of fit

In previous studies, theoretical models have been fit to experimental SAXS data by comparison in q-space (37,38). In a similar fashion we compute quality of fit as the root-mean square (RMS) error (i.e., the square root of the sum of the point-by-point squared errors between experimental and simulated structure factors) averaged over all six dsDNA lengths,

$$\frac{1}{N_{\text{lengths}}}\sum_{\text{dsDNA lengths}}\sqrt{N^{-1}\sum_{i}^{N}\left[S_{\text{exp}}(q_i)-S_{\text{sim}}(q_i)\right]^2}$$

Here $S_{\text{exp}}(q_i)$ and $S_{\text{sim}}(q_i)$ are the values of the experimental and simulated structure factors, respectively, sampled at N equally spaced wavevectors q_i. We found the best fit for our experiments with a WLC model with a persistence length of 70 nm. However, the experiment is not especially discriminating among persistence lengths in the broad vicinity of this value: persistence lengths of 50–100 nm had RMS error within 8% of the minimum at 70 nm. The fit for $\ell_P = 50$ nm gives a good approximation to the means and variances across the different lengths of dsDNA (Figs. 5 and 6). Greater discriminatory power could be achieved with access to a wider range of scattering angles, as some structural information for systems of our size is lost when low-wavevector scattered intensity is blocked by the beamstop. Nevertheless, these results strongly suggest that 50 nm WLC reasonably captures equilibrium dsDNA bending elasticity down to chains as short as ~40 bp.

Nonlinear elasticity does not impact these results

Polymer models as schematic as the WLC are often reserved for chains well in excess of ℓ_P in length. It is generally true that microscopic details remain important up to the length scale on which correlations in the corresponding fluctuations decay. That idea does not, however, contradict the success of WLC descriptions we report. A common orientation of two chain segments does not imply correlations between their internal structures, which determine the degree of local bending. The more rapid decay of these latter correlations, associated with fluctuations in internal structure, sets the length scale on which a simple bending potential lacking molecular details can become appropriate.

Consider a chain that is only marginally flexible but nonetheless comprises many independently bending nodes. The potential energy $u(\kappa_i)$ governing bending at each node may be complicated but we require it to depend only upon the magnitude $|\kappa_i|$ of local curvature (ensuring that $\kappa = 0$ on average). In this example the curvatures $\kappa_i = \hat{t}_{i+1} - \hat{t}_i$ are statistically independent random variables distributed as

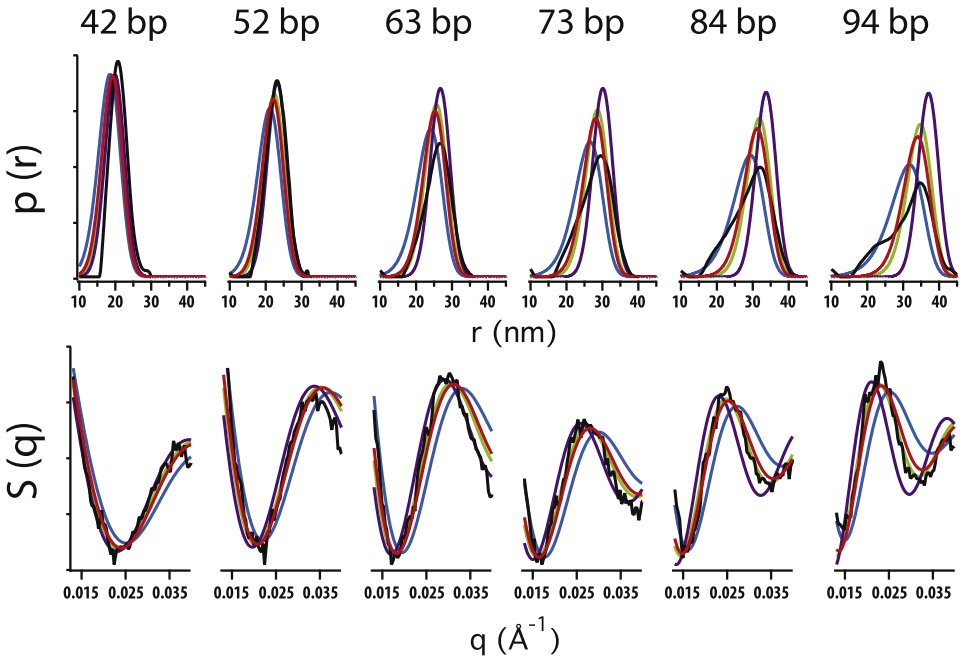

FIGURE 5 Comparison of experimental structure factors and pair distribution functions (*black curves*) with simulations for WLC models with 25 nm (*blue curves*), 50 nm (*red curves*), 70 nm (*green curves*), and infinite (*purple curves*) persistence lengths. Artifacts from indirect Fourier transformation are apparent in the shoulder in the real-space $p(r)$ for the 94-bp construct.

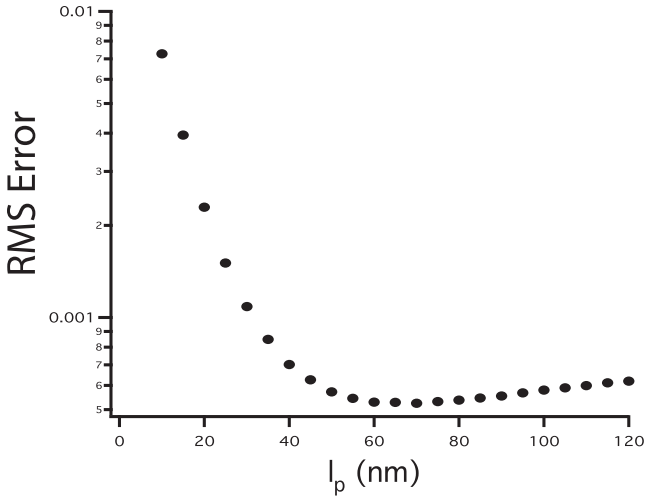

FIGURE 6 RMS error, averaged over all six strand lengths, between experimental distributions and distributions from WLC dsDNA for different persistence lengths.

$$p(\kappa_i) \propto \exp[-\beta u(\kappa_i)],$$

where $\beta = (k_B T)^{-1}$.

In the specific case of a WLC, $u \propto |\kappa_i|^2$, so that κ_i values are Gaussian random variables. Suppose we now take a coarser view of bending, comparing the chain's orientation at node i with that at node $i + n$. Correspondingly, we define a coarse-grained curvature

$$\overline{\kappa}_i^{(n)} = \hat{t}_{i+n} - \hat{t}_i,$$

and note that $\overline{\kappa}_i^{(n)}$ is simply a sum of many κ_i values, i.e.,

$$\overline{\kappa}_i^{(n)} = \sum_{j=i}^{i+n-1} \kappa_i.$$

The effective potential $\overline{u}$ governing fluctuations in $\overline{\kappa}_i^{(n)}$ could be determined from an n-fold convolution of $p(\kappa_i)$. The central limit theorem dictates that as $n \to \infty$, the resulting statistics of $\overline{\kappa}_i^{(n)}$ become Gaussian, regardless of the details of $u(\kappa_i)$. This convergence should be quite rapid for the range of $\overline{\kappa}_i^{(n)}$ accessible in the course of typical fluctuations, especially if $p(\kappa_i)$ itself bears some resemblance to a Gaussian distribution. As a consequence, we expect $\overline{u} \propto |\overline{\kappa}_i^{(n)}|^2$ to be a good approximation even for modest n. A small number of statistically independent segments thus behave collectively much as a WLC. A very similar conclusion has been drawn by more rigorous (but also more complicated) means by Wiggins et al. (39).

As an illustration of this rapid convergence to WLC mechanics, we considered a specific example anharmonic bending energy, originally developed by Yan and Marko to rationalize short-length scale dsDNA cyclization experiments (40). Each node has two internal states, notionally corresponding to hybridized and melted local structures. These states differ both in energy (the molten state of an unbent node lies higher in energy by an amount $\Delta\mu$) and in bending stiffness (characterized by two persistence lengths, $\ell_P^{melt} < \ell_P$ and $\ell_P^{hybrid} > \ell_P$).

Consistency with the observed large-scale elasticity of DNA, ($\ell_P \approx 50$ nm) imposes a relationship among these parameters. For a discrete chain the persistence length can be expressed as a function of the average cosine of the bending angle at each node, $\langle \cos\theta \rangle$, as $\ell_P = \frac{d}{1-\langle \cos\theta \rangle}$. For a meltable chain, the average cosine is simply linearly averaged over both melts and hybridized dsDNA according to their respective statistical weights, leading immediately to an effective persistence length

$$\ell_p^{eff} = \frac{1 + e^{\beta\mu}}{\frac{e^{-\beta\mu}}{\ell_p^{melt}} + \frac{1}{\ell_p^{hybrid}}}.$$

We have considered a very flexible molten state ($\ell_p^{melt} = 2.5$ nm) and values of $\Delta\mu$ ranging from 3 to 12 $k_B T$. The lower limit of this range requires almost complete rigidity of the hybridized state to maintain the appropriate large-scale persistence length, representing the strongly anharmonic bending potential of a node that is alternately very permissive and very prohibitive of bending fluctuations. At the upper limit of the $\Delta\mu$ range, melting is so infrequent as to be inconsequential for typical equilibrium fluctuations.

We held fixed the persistence length of melted dsDNA ℓ_p^{melt} at 2.5 nm (the overall trend remained for 1.5 and 3.5 nm as well), varied $\Delta\mu$, and adjusted the persistence length of hybridized dsDNA ℓ_p^{hybrid} to maintain an effective persistence length of 50 nm, equal to the well-established value from single-molecule force-extension experiments. For each set of these parameters we computed end-to-end distributions of short chains. With the constraint outlined above, regardless of the value of melt free energy $\Delta\mu$, a similar distribution emerged. Indeed, this pattern proved to be general: for a given effective persistence length (we tried 20, 30, 40, and 50 nm; 50 nm displayed), the dsDNA end-to-end distance distributions are essentially insensitive to melt free-energies ranging from 5 to 12 $k_B T$ (Fig. S7 *C*). This insensitivity to melting degrees of freedom only begins to break down for very facile melts ($\Delta\mu \lesssim 3\ k_B T$), or for very short chains ($\lesssim$10 bp, not shown). However, the corresponding melt statistics for a model with $\Delta\mu \lesssim 3\ k_B T$ are inconsistent with calorimetry and UV melting experiments (30). We also note that a subelastic chain (39), with

$$E_{bend} = \sum_{\text{basepairs } i} B\theta_i^2$$

and B chosen to give $\ell_P = 50$ nm, also gives essentially indistinguishable end-to-end distributions.

CONCLUSIONS

In this work, we have explored a new method for studying structural fluctuations in biomacromolecules by decorating

them with gold nanoparticle markers. SAXS measurements on these constructs report on distributions of interparticle distance, which in the case of dsDNA, reflect thermal bending fluctuations of the double helix. By comparing with computer simulations of models for DNA elasticity, we determined that conventional WLC descriptions developed for large-scale mechanics remain suitable even for sub-persistence length oligomers. Good agreement, which requires a detailed treatment of the gold-DNA junction, suggests that the length scale associated with correlated bending fluctuations spans no more than a handful of bp. This conclusion is robust to moderate changes in DNA sequence and ionic strength.

A recent study (41) examined SAXS of gold nanoparticles tethered by shorter dsDNA chains (10–35 bp). Inferred gold-gold distance distributions were significantly broader and more symmetric than expected from bending fluctuations alone, leading the authors to conclude that stretching is the dominant source of distance fluctuations for their short constructs. They posited a compliance to stretch much higher than previously believed, and a cooperativity of stretch fluctuations, to reproduce the experimentally observed variances in gold-gold distance. Our alkane linkers and dsDNA chains are each significantly longer than those used in their experiments, and thus linker fluctuations and DNA bending fluctuations should each play a more significant role in our experiments. We have adapted our simulations, which lack stretch fluctuations altogether, to examine the constructs studied in their work, simply by changing the parameters characterizing nanoparticle size and linker length. Our computed distributions of gold-gold distances exhibit variances as large or larger than those inferred in Mathew-Fenn et al. (41) from SAXS data, due primarily to flexibility of the alkane linkers.

The experimental strategy we have pursued can serve broadly as a quantitative alternative to approaches like fluorescence resonance energy transfer for characterizing equilibrium variations in microscopic structure. In the context of DNA mechanics, further experiments could be performed on systems we deliberately avoided: DNA with A-tracts, DNA with mismatches or hairpins, or even DNA bound by proteins or saturated with intercalating agents such as platinum complexes. More generally, this approach is well suited to examine nanometer-scale fluctuations in a variety of soft materials, such as proteins.

SUPPORTING MATERIAL

Seven figures and one table are available at http://www.biophysj.org/biophysj/supplemental/S0006-3495(09)01165-5.

Steve Whitelam and Shelley A. Claridge provided useful discussion.

A.J.M. acknowledges funding from the United States Department of Energy. D.A.S. acknowledges support from a National Science Foundation Graduate Research fellowship. This work was supported by the Director, Office of Science, Office of Basic Energy Sciences, of the U.S. Department of Energy under contract No. DE-AC02-05CH11231.

REFERENCES

1. Garcia, H. G., P. Grayson, L. Han, M. Inamdar, J. Kondev, et al. 2007. Biological consequences of tightly bent DNA: the other life of a macromolecular celebrity. *Biopolymers*. 85:115–130.
2. Sherman, W., and N. Seeman. 2006. Design of minimally strained nucleic acid nanotubes. *Biophys. J*. 90:4546–4557.
3. Mirkin, C., R. Letsinger, R. Mucic, and J. Storhoff. 1996. A DNA-based method for rationally assembling nanoparticles into macroscopic materials. *Nature*. 382:607–609.
4. Fu, A., C. M. Micheel, J. Cha, H. Chang, H. Yang, et al. 2004. Discrete nanostructures of quantum dots/Au with DNA. *J. Am. Chem. Soc*. 126:10832–10833.
5. Claridge, S. A., S. L. Goh, J. M. J. Frechet, S. C. Williams, C. M. Micheel, et al. 2005. Directed assembly of discrete gold nanoparticle groupings using branched DNA scaffolds. *Chem. Mater*. 17:1628–1635.
6. Aldaye, F. A., and H. F. Sleiman. 2007. Dynamic DNA templates for discrete gold nanoparticle assemblies: control of geometry, modularity, write/erase and structural switching. *J. Am. Chem. Soc*. 129:4130–4131.
7. Claridge, S. A., A. J. Mastroianni, Y. B. Au, H. W. Liang, C. M. Micheel, et al. 2008. Enzymatic ligation creates discrete multinanoparticle building blocks for self-assembly. *J. Am. Chem. Soc*. 130:9598–9605.
8. Mastroianni, A. J., S. A. Claridge, and A. P. Alivisatos. 2009. Pyramidal and chiral groupings of gold nanocrystals assembled using DNA scaffolds. *J. Am. Chem. Soc*. 131:8455–8459.
9. Reinhard, B., S. Sheikholeslami, A. Mastroianni, A. P. Alivisatos, and J. Liphardt. 2007. Use of plasmon coupling to reveal the dynamics of DNA bending and cleavage by single *Eco*RV restriction enzymes. *Proc. Natl. Acad. Sci. USA*. 104:2667–2672.
10. Bustamante, C., S. Smith, J. Liphardt, and D. Smith. 2000. Single-molecule studies of DNA mechanics. *Curr. Opin. Struct. Biol*. 10:279–285.
11. Bustamante, C., Z. Bryant, and S. Smith. 2003. Ten years of tension: single-molecule DNA mechanics. *Nature*. 421:423–427.
12. Crothers, D., J. Drak, J. Kahn, and S. Levene. 1992. DNA bending, flexibility, and helical repeat by cyclization kinetics. *Methods Enzymol*. 212:3–29.
13. Yuan, C., H. Chen, W. L. Xiong, and L. A. Archer. 2008. DNA bending stiffness on small length scales. *Phys. Rev. Lett*. 100:018102.
14. Cloutier, T., and J. Widom. 2004. Spontaneous sharp bending of double-stranded DNA. *Mol. Cell*. 14:355–362.
15. Du, Q., C. Smith, N. Shiffeldrim, M. Vologodskaia, and A. Vologodskii. 2005. Cyclization of short DNA fragments and bending fluctuations of the double helix. *Proc. Natl. Acad. Sci. USA*. 102:5397–5402.
16. Wiggins, P., T. van der Heijden, F. Moreno-Herrero, A. Spakowitz, R. Phillips, et al. 2006. High flexibility of DNA on short length scales probed by atomic force microscopy. *Nat. Nanotechnol*. 1:137–141.
17. Wang, L. X., and V. A. Bloomfield. 1991. Small-angle x-ray scattering of semidilute rodlike DNA solutions—polyelectrolyte behavior. *Macromolecules*. 24:5791–5795.
18. Koch, M. H. J., Z. Sayers, P. Sicre, and D. I. Svergun. 1991. A synchrotron radiation electric field x-ray solution scattering study of DNA at very low ionic strength. *Macromolecules*. 28:4904–4907.
19. Koch, M. H. J., P. Vachette, and D. I. Svergun. 2003. Small-angle scattering: a view on the properties, structures and structural changes of biological macromolecules in solution. *Q. Rev. Biophys*. 36:147–227.
20. Zanchet, D., C. M. Micheel, W. J. Parak, D. Gerion, and A. P. Alivisatos. 2001. Electrophoretic isolation of discrete Au nanocrystal/DNA conjugates. *Nano Lett*. 1:32–35.
21. Zanchet, D., C. M. Micheel, W. J. Parak, D. Gerion, S. C. Williams, et al. 2002. Electrophoretic and structural studies of DNA-directed Au nanoparticle groupings. *J. Phys. Chem. B*. 106:11758–11763.
22. Bloomfield, V. A., D. M. Crothers, and I. Tinoco. 2000. Nucleic Acids: Structures, Properties, and Functions. University Science Books, Sausalito, CA.

23. Claridge, S. A., H. W. Liang, S. R. Basu, J. M. J. Frechet, and A. P. Alivisatos. 2008. Isolation of discrete nanoparticle-DNA conjugates for plasmonic applications. *Nano Lett*. 8:1202–1206.

24. Glatter, O. 1977. A new method for the evaluation of small-angle scattering data. *J. Appl. Cryst*. 10:415–421.

25. Svergun, D. 1992. Determination of the regularization parameter in indirect-transform methods using perceptual criteria. *J. Appl. Cryst*. 25:495–503.

26. Segall, D. E., P. C. Nelson, and R. Phillips. 2006. Volume-exclusion effects in tethered-particle experiments: bead size matters. *Phys. Rev. Lett*. 96:088306.

27. Markham, N. R., and M. Zuker. 2005. DINAMelt web server for nucleic acid melting prediction. *Nucleic Acids Res*. 33:W577–W581.

28. Boal, D. H. 1991. Mechanics of the Cell. Cambridge University Press, Cambridge, UK.

29. Olson, W., A. Gorin, X. Lu, L. Hock, and V. Zhurkin. 1998. DNA sequence-dependent deformability deduced from protein-DNA crystal complexes. *Proc. Natl. Acad. Sci. USA*. 95:11163–11168.

30. SantaLucia, J. 1998. A unified view of polymer, dumbbell, and oligonucleotide DNA nearest-neighbor thermodynamics. *Proc. Natl. Acad. Sci. USA*. 95:1460–1465.

31. Crothers, D., T. Haran, and J. Nadeau. 1990. Intrinsically bent DNA. *J. Biol. Chem*. 265:7093–7096.

32. MacDonald, D., K. Herbert, X. Zhang, T. Polgruto, and P. Lu. 2001. Solution structure of an A-tract DNA bend. *J. Mol. Biol*. 306:1081–1098.

33. Davis, J. T. 2004. G-quartets 40 years later: from 5′-GMP to molecular biology and supramolecular chemistry. *Angew. Chem. Int. Ed*. 43:668–698.

34. Baumann, C., S. Smith, V. Bloomfield, and C. Bustamante. 1997. Ionic effects on the elasticity of single DNA molecules. *Proc. Natl. Acad. Sci. USA*. 94:6185–6190.

35. Qiu, X. Y., L. W. Kwok, H. Y. Park, J. S. Lamb, K. Andersen, et al. 2006. Measuring inter-DNA potentials in solution. *Phys. Rev. Lett*. 96:138101.

36. Qiu, X. Y., K. Andersen, L. W. Kwok, J. S. Lamb, H. Y. Park, et al. 2007. Inter-DNA attraction mediated by divalent counterions. *Phys. Rev. Lett*. 99:038104.

37. Hura, G., J. M. Sorenson, R. M. Glaeser, and T. Head-Gordon. 2000. A high-quality x-ray scattering experiment on liquid water at ambient conditions. *J. Phys. Chem*. 133:9140–9148.

38. Sorenson, J. M., G. Hura, R. M. Glaeser, and T. Head-Gordon. 2000. A high-quality x-ray scattering experiment on liquid water at ambient conditions. *J. Phys. Chem*. 133:9149–9161.

39. Wiggins, P. A., and P. C. Nelson. 2006. Generalized theory of semiflexible polymers. *Phys. Rev. E Stat. Nonlin. Soft Matter Phys*. 73:031906.

40. Yan, J., and J. F. Marko. 2004. Localized single-stranded bubble mechanism for cyclization of short double helix DNA. *Phys. Rev. Lett*. 93:108108.

41. Mathew-Fenn, R., R. Das, and P. Harbury. 2008. Remeasuring the double helix. *Science*. 322:446–449.